



AUTHOR(S):

TITLE:

YEAR:

Publisher citation:

OpenAIR citation:

Publisher copyright statement:

This is the _____ version of an article originally published by _____
in _____
(ISSN _____; eISSN _____).

OpenAIR takedown statement:

Section 6 of the "Repository policy for OpenAIR @ RGU" (available from <http://www.rgu.ac.uk/staff-and-current-students/library/library-policies/repository-policies>) provides guidance on the criteria under which RGU will consider withdrawing material from OpenAIR. If you believe that this item is subject to any of these criteria, or for any other reason should not be held on OpenAIR, then please contact openair-help@rgu.ac.uk with the details of the item and the nature of your complaint.

This publication is distributed under a CC _____ license.

1 **Rate-Dependent Polymer Adsorption in Porous Media.**

2 **P.E.G. Idahosa*, G.F. Oluyemi, M. B. Oyeneyin, and R. Prabhu.**

3 School of Engineering, Robert Gordon University, Riverside East, Garthdee Road, Aberdeen,
4 AB10 7GJ, United Kingdom.

5 *Address all correspondence to: *P.E.G. Idahosa*, School of Engineering, *Robert Gordon*
6 *University, Riverside East, Garthdee Road, Aberdeen, AB10 7GJ, United Kingdom.*

7 *Tel: +44 (0) 1224262451, E-mail: p.e.g.idahosa@rgu.ac.uk*

8

9 **Abstract**

10 Laboratory core flood experiments were conducted at different flow rates with partially
11 hydrolysed polyacrylamide (HPAM) oilfield Enhanced Oil Recovery (EOR) polymer and
12 silica sand to investigate the polymer retention in porous media due to flow rate variation.
13 Specifically, the double-polymer bank method was used in a new way to quantify and
14 understand total incremental retention (both reversible and irreversible) induced by flow rate
15 variation for HPAM polymers. Experimental results indicate that adsorption was the
16 dominant retention mechanism. Further, the results obtained show that polymer adsorption
17 was rate-dependent (i.e., as flow rate increased, adsorption increased), and that the adsorption
18 was largely reversible with minimal incremental irreversible adsorption. It was also observed
19 that flow rate impacted polymer inaccessible pore volume (IAPV), decreasing from 32% to
20 15% as flow rate increased from 0.8 ml/min to 6.0 ml/min. Finally, results from the study
21 also give better insight into understanding HPAM flow-induced adsorption and their effect on
22 permeability reduction processes.

23

24 **Keywords:** Polymer adsorption, Core flooding, Enhanced oil recovery, Porous media, Flow
25 rate.

1 **1. Introduction**

2 Polymer flooding has been widely used as an attractive alternative to conventional water
3 flooding in Enhanced oil Recovery (EOR) and in oilfield water and gas shut-off. The main
4 objectives being to increase the oil recovery factor by decreasing the mobility between the
5 displacement (water) and displaced (oil) fluids (Lake et al., 2014). However, Polymer
6 retention and inaccessible pore volume (IAPV) are the two components that govern polymer
7 propagation through porous media in the dynamic mode. It is also widely recognised that
8 when polymer solutions interact with a solid surface, the polymer molecules may be retained
9 on the solid surface by both the physical forces of van der Waal's and hydrogen bonding
10 forces (Dang et al., 2014). Retention refers to all mechanisms that remove polymer from the
11 transported aqueous phase. These include: adsorption, mechanical entrapment (Yerramilli et
12 al., 2013) and hydrodynamic (or rate) retentions (Chauveteau et al., 2002). However, a survey
13 of the literature reveals that only a few studies have investigated the variation of polymer
14 retention with flow rates (Maerker, 1973; Dominguez and Willhite, 1977; Huh et al., 1990;
15 Aubert and Tirrell, 1980; Chauveteau et al., 2002). For example, using 100 to 300 mD Berea
16 cores at residual oil saturation, Huh et al. (1990) showed that xanthan retention was only
17 about 6% greater at 1 ft/d than at 0.333 ft/d. Using different xanthan solution in similar cores
18 in a separate experiment, the same authors observed that the retained polymer was 40% more
19 at 5 ft/d than at 1 ft/d. In a similar manner, Maerker (1973) showed some evidence of xanthan
20 retention in a 121 md Berea core as the fluid velocity was increased and proposed that the
21 higher pressure gradient resulting from the increased fluid velocity caused the deformation of
22 the xanthan molecules which got trapped within the core in relatively smaller pores. Maerker
23 further argued that as flow reduced, the molecules relaxed to a random coil and then diffused
24 to larger pore channels, causing temporary increase in polymer concentration until the excess
25 polymer was flushed from the core. Using Pusher 700 and 86-mD core made of compacted

1 Teflon powders, Dominguez and Willhite (1977) showed that flow rate affects polymer
2 retention and that nearly all retention could be attributed to mechanical entrapment because
3 of the low polymer adsorption on the Teflon surface. These reversible occurrences have been
4 described as hydrodynamic retention. However, most of these previous works used xanthan
5 gum in their studies. The permeability reduction factor is not significant for many polymers
6 such as xanthan gum or when the formation permeability is very high (Lake et al., 2014). The
7 above literature survey shows that these previous works have not generally explored the
8 correlation between the magnitude of polymer retention and flow rate; and specifically
9 therefore, the effect of flow rate on HPAM polymer retention have not been fully quantified.
10 In this paper, the focus is on single phase linear polymer core displacement experiments
11 using HPAM polymers with natural sand pack; and the data generated were analysed by a
12 special method to quantify the effect of flow rate on HPAM polymer adsorption and their
13 impact on permeability reduction. The method also enables the differentiation of total
14 incremental polymer retention in terms of “reversible” and “irreversible” adsorption induced
15 by flow rate variation.

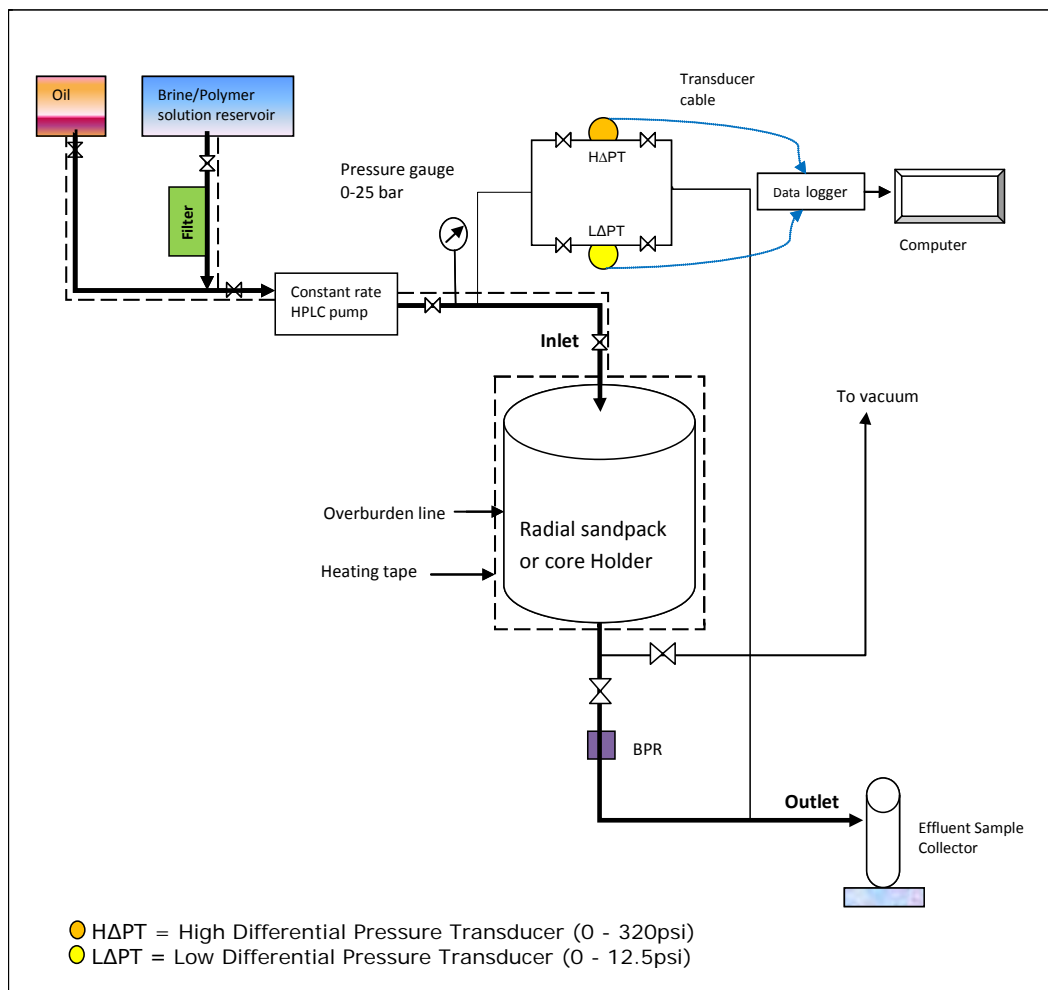
16

17 **2. Experimental Implementation**

18 **2.1 Materials and methods**

19 **Fig. 1** shows a simplified schematic of the core flood experimental rig setup in which the
20 important and required key equipment are indicated. In the dynamic flow system, lines and
21 valves are set up to minimise dead volumes in which fluids can be lost. The coreflood rig
22 setup for the polymer flooding experiments consisted of a stainless steel radial core or
23 sandpack holder designed in-house to simulate reservoir radial flow. However, the sandpack
24 core holder was operated as a linear flow model during the core flooding with inlet from top
25 and outlet from bottom. In **Fig. 1**, a high performance syringe pump (model HPLC 1500) was

1 used to deliver a varying, pre-defined fluid volume at constant injection or flow rate across
2 the core sample. The pump (which has a maximum pressure of 6000 psi and can deliver to
3 12.00 ml/min) was used to provide a non-pulsating flow during the experiment. All in-place
4 pressure monitoring and measurements were electronic and digitised with the aid of a high-
5 speed National Instruments data acquisition system (NIDAQ) through Validyne pressure
6 transducers of varying capacities mounted across the core and a personal computer. Low (0-
7 12.5 psi) and high (0-320 psi) capacity transducers were chosen according to the pressure
8 range and the requirements of the measurement resolution. A Validyne carrier demodulator
9 model CD223 (manufactured by Validyne Engineering, USA) was used to provide the correct
10 sensor excitation and demodulate the returned Alternating Current (AC) signal from the
11 sensors into a +/-10 Vdc signal appropriate for the data acquisition input. The CD223 accepts
12 two transducer inputs but the display and signal follow a front panel switch so that the
13 readings from only one sensor at a time are displayed. As the analog output follows the
14 display, it was not possible to record both transducer readings simultaneously. Furthermore,
15 an absolute pressure gauge (0-360 psi) was mounted at the pump outlet in order to monitor
16 inlet pressure and avoid over-pressuring the flow system.



1

2 Fig. 1. Schematic of experimental setup for the implementation of the dynamic polymer
3 coreflood.

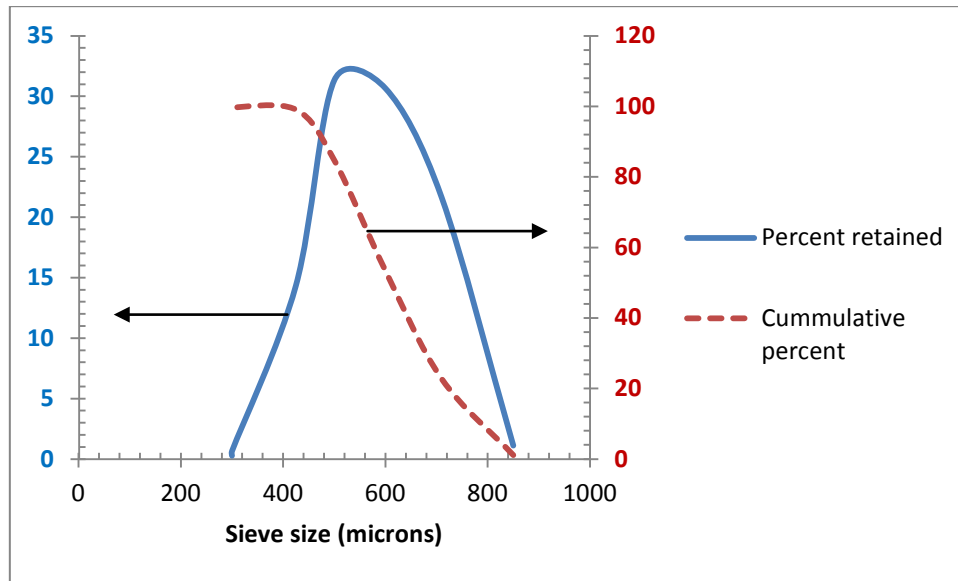
4

5 2.1.1 Porous Media Description.

6 Commercial grade silica sand (20/40 mesh size) was used to make the sand pack in the
7 experiments. Their interactions with polymer molecules in solutions as well as with salts are
8 quite comparable to those of natural sands (Zitha et al., 1995). Also, the possibility of
9 hydrogen bond formation with silica has been proposed to explain the high affinity of
10 polymers for many reservoir rocks (Pefferkorn et al., 1985). **Fig. 2** and **Table 1** show the
11 results of the analysis of the grain size distributions of the sand done by direct sieving of the

1 sample. Optical microscopy (using Leica DFC420 Digital Microsystems) was used to capture
2 high-resolution images of the silica sands for shape identification. The sand was observed to
3 be spherical in shape as shown in **Fig. 3**. The geometry of this type of shape enables its
4 porosity to be calculated.

5



6

7 Fig. 2. Individual (*continuous lines*) and cumulative (*dashed lines*) percent retained for the
8 20/40 silica sand

9

10

11

12

13

14

15

16

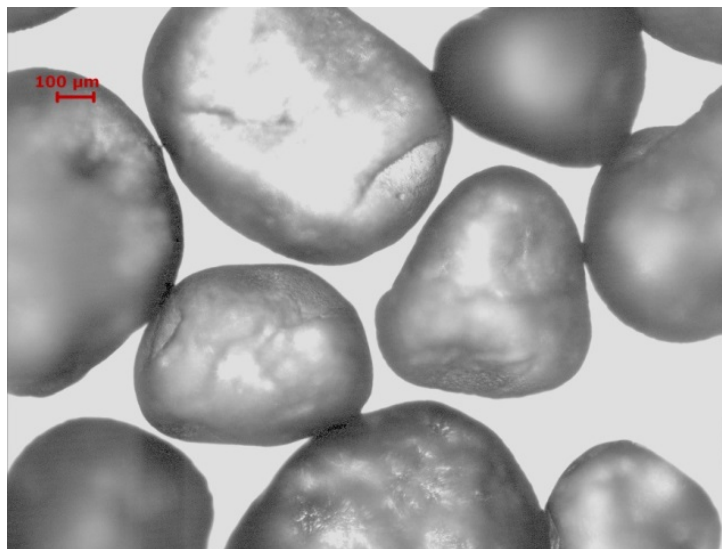
17

18

1 Table 1. Characteristics of the 20/40 silica sand used in this study.

<i>Typical physical properties of the 20/40 sand size</i>			
Colour	White	Mineral	Quartz
Grain shape	Round	Bulk density	1.54 g/cc
Hardness (Mohs)	7	Specific gravity	2.65 g/cc
Melting point (⁰ F)	150	pH	7
<i>Typical chemical analysis</i>			
Silicon Dioxide (SiO ₂)	99.5+	Magnesium Oxide (M _g O)	<0.01
Aluminium Oxide (Al ₂ O ₃)	0.06	Sodium Oxide (Na ₂ O)	<0.01
Iron Oxide (Fe ₂ O ₃)	0.02	Potassium Oxide (K ₂ O)	<0.01
Titanium Oxide (TiO ₂)	0.012	Loss on Ignition (LOI)	0.1
Calcium Oxide (CaO)	<0.01		

2



3

4 Fig. 3. Microscopic image of the 20/40 Silica sand (5x Objective magnification).

5

6 The sand was dry-packed in radial core holder with length of 2.28 cm, internal diameter of
 7 4.40 cm, cross-sectional area of 15.21 cm², and internal volume of 34.67 cm³. The sand
 8 material loaded into the holder was weighed and recorded. The volume of the sand material
 9 was determined accurately from knowledge of the grain density. The pore volume of the

1 porous media was then calculated using the direct method (i.e. by subtracting the volume of
 2 the sand material in the holder from the bulk volume). The porosity was thereafter
 3 determined from the pore volume and bulk volume data. After the sample's pore volume and
 4 porosity measurements, the brine absolute permeability was experimentally determined for
 5 the porous media. In computing absolute permeability, measurements at different flow
 6 conditions were obtained so that an average value for permeability can be calculated as well
 7 as detect presence of gas saturation. The pressure differentials (measured with the aid of
 8 pressure transducers) were noted and recorded for the different flow rates used after steady-
 9 state conditions were reached, i.e., a constant flow rate was attained at a constant pressure
 10 differential. Core absolute permeability to brine from the pressure and flow rate data (plotted
 11 as **Fig. 4**) was calculated using Darcy's law (Eqn. (1):

$$12 \quad k_b = \frac{q \mu_{app} \cdot L}{A \cdot \Delta P} \quad (1)$$

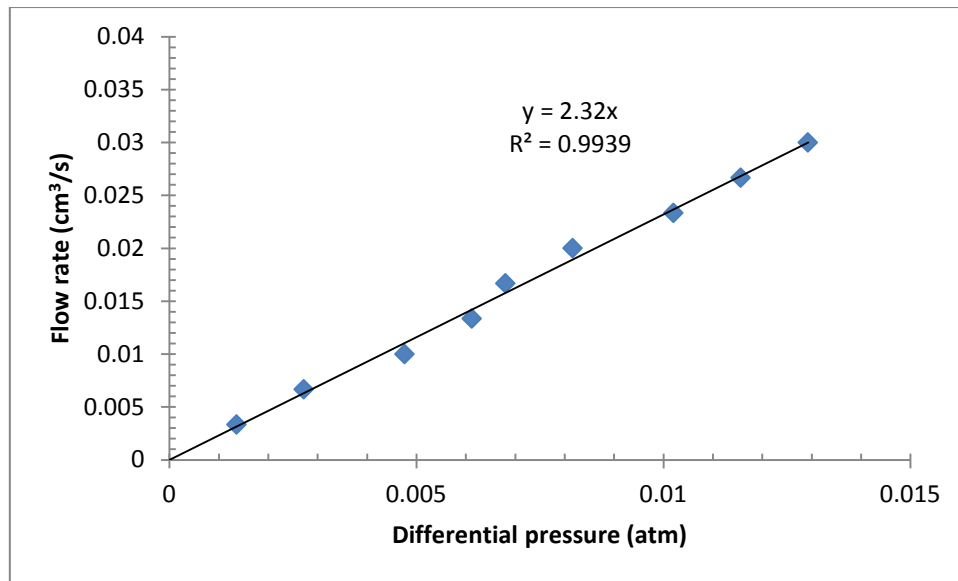
13 where, k_b = permeability to brine, Darcies; μ_{app} = apparent fluid viscosity, cp; ΔP = pressure
 14 drop across length L, atm; q = volumetric flow rate, cm³/s; A = cross-sectional area of core,
 15 cm²; L = length of core, cm.

16

17 A straight line through the origin was then fitted to the plot of q vs. ΔP by the no-intercept
 18 regression model (Abu-Khamsin, 2004) as shown in **Fig. 4**. The slope (m) of this straight line
 19 is the core sample's permeability multiplied by $A/\mu L$, i.e. Eqn. (2). **Table 2** shows the
 20 petrophysical properties of the sand.

$$21 \quad k = \frac{m \mu L}{A} \quad (2)$$

22



1

2 Fig. 4. Plot of flow rate against differential pressure

3

4 Table 2. Petrophysical properties of the 20/40 silica sand used in this study.

Sieve mesh	Particle size range, μm	Average particle diameter, μm	Porosity, fraction	Permeability, mD	Pore vol, ml	Dia., cm	Area, cm^2
20/40	300-850	564	0.372	348.8	12.93	4.40	15.21

5

6 2.1.2 Polymers

7 Commercial grade partially Hydrolysed Polyacrylamide (HPAM) was used in all
 8 experiments. The HPAM (SNF Flopaam 3630 S) was manufactured and kindly provided in
 9 powder form by SNF Floerger, ZAC de Milieux, 42163 Andrezieux, France. In order to
 10 ensure optimum solution properties, the polymer was mixed in strict compliance with the
 11 recommended procedures provided by the manufacturers and in accordance with API RP 63
 12 (1990) guidance.

13

14

1 2.1.3 Brine

2 3.2% TDS synthetically formulated brines (SFB) was made to mimic reservoir waters.
3 Sodium chloride (NaCl), anhydrous calcium chloride (CaCl₂), potassium chloride (KCl),
4 sodium hydrogen carbonate (NaHCO₃) and magnesium chloride hexahydrate (MgCl₂.6H₂O)
5 were the analytical reagents used to prepare the brine. The concentration of each salt in the
6 synthesised brine is shown in **Table 3**. The brine has ionic strength of 0.608 calculated from
7 ionic composition of the salts using Eqn. (3):

$$8 \quad I = \frac{1}{2} \cdot \sum C_i \cdot Z_i^2 \quad (3)$$

9 where, I = Ionic strength, C_i = concentration of the i th species (mole/L), Z_i = valence (or
10 oxidation) number of the i th species.

11

12 Prior to their use in all flow experiments, the brine solutions were filtered with 0.22 μ m filter
13 paper. This was done to ensure that no particles interfered with the reliable operation of the
14 pump piston seals and check valves; and prevent undue pore blockage during core tests. 2.0
15 g/L commercial formaldehyde was added to the brine as oxygen scavenger, biocide or
16 bactericide and stabilizer against free radical depolymerisation. For the core flooding tests, all
17 polymer solutions were prepared as “*smart*” solutions as they were spiked with 0.004M
18 (0.034%) sodium bicarbonate to counteract undesired pH changes in adsorption experiments.
19 The bicarbonate buffered against an acidic reaction when silica contacted water and against
20 an alkaline reaction with calcium carbonate. The brine to which 2.0 g/L commercial
21 formaldehyde (to act as oxygen scavenger, biocide or bactericide and stabilizer against free
22 radical depolymerisation) was added in deionised water was the same as that used for
23 preparing the polymer solutions. To ensure flow rate consistency, the brine and polymer
24 solutions were doubly evacuated using both ultrasonic and helium degassing. Specifically,

1 after sonicating, the solvents were then sparged with 99.99⁺ % standard laboratory grade
2 helium. Helium presents the best practical technique for degassing because it is only
3 sparingly soluble in HPLC solvents, so other gases dissolved in the solvent diffuse into the
4 helium bubbles and are swept away from the system. The solutions were continually
5 blanketed with the helium during use to keep atmospheric gases from dissolving back into the
6 mobile phase.

7

8 Table 3. Chemical composition of the artificially formulated brine

Compound	NaCl	CaCl ₂	KCl	NaHCO ₃	MgCl ₂ .6H ₂ O
Concentration (g/L)	26.4	1.18	0.40	7.34	5.27

9

10 2.2 Experimental procedure

11 Polymer retention was first measured at low flow rate of 0.8 ml/min using the double-
12 polymer bank dynamic method proposed by Lotsch et al. (1985), Hughes et al. (1990),
13 Osterloh and Law (1998). Specifically, the following procedure was followed:

- 14 1) 3.2% TDS brine was injected at fixed low rate of 0.8 ml/min until stabilisation. This sand
15 conditioning step enables the achievement of stabilised baselines of viscosity and spectral
16 absorbance for the effluent from the sandpacks.
- 17 2) About 2.5 PV of 500 ppm SNF Flopaam 3630 S HPAM solution (in 3.2% TDS brine)
18 was injected also at fixed low rate of 0.8 ml/min. This is the first low rate polymer
19 injection cycle.
- 20 3) Subsequently, 130 ml (about 10 PV) of brine was injected to flush all non-adsorbed
21 polymers from the core.
- 22 4) Then, step (2) was repeated (this is the second low rate polymer injection cycle).
- 23 5) Step 3 was repeated.

- 1 6) When effluents concentration reached injected concentration, samples were periodically
2 collected in small pore volume (PV) increments for polymer-concentration determination
3 using the viscosity method by reading and converting capillary viscometer efflux times.
4 Note: 1 PV in this case is 12.93 cm³.
- 5 7) Pressure drops during steps 3 and 5 were recorded and (if required) used to calculate
6 residual resistance factor (RRF); by dividing the pressure drop at these stages by that
7 measured in step 1.
- 8 8) Polymer retention was calculated by comparing polymer effluent curves in steps 2 and 4
9 (i.e., by plotting two effluent polymer-concentration profiles vs. pore volumes (PV)
10 injected.

11

12 **2.3 Special method to detect flowrate-dependent retention**

13 To study and quantify the influence of flowrate on retention after measuring retention at low
14 flow rate of 0.8 ml/min, two equal and identical banks of polymer solutions were injected
15 each at fixed high rates of 3 ml/min and 6 ml/min through the same core or sand pack of
16 similar properties as was done for the low rate retention determination. The same procedure
17 as the low rate retention determination was followed. This double-polymer/tracer-bank
18 dynamic method also allowed for the determination of IAPV due to rate variation.

19

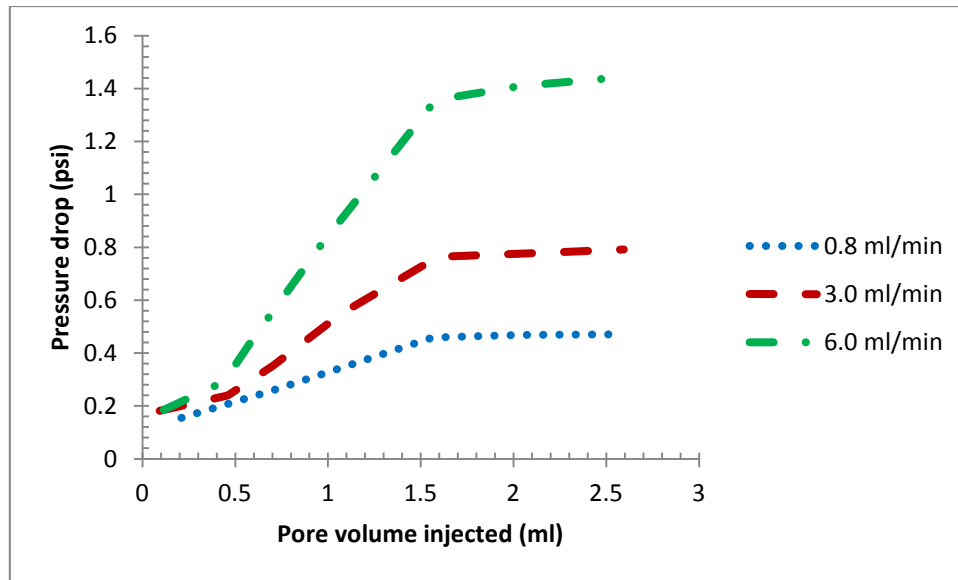
20 **3. Results and Discussion.**

21 **3.1 Effect of flow rates on pressure behaviour**

22 The effect of different flow rates on pressure behaviour during the polymer displacement is
23 shown in **Fig. 5**. Due to the nature of the short plugs used, it is noticeable that the pressure
24 increase for each flow rate is small; with the 0.8 ml/min case having the less impact on the
25 pressure drop. However, as the polymer enters the core, the pressure rises, and continues to
26 do so as more pore volumes are injected. This increase in pressure is attributable to adsorbed
27 polymer layer and/or polymer and brine passage through the core. It is further observed that

1 the pressure drop stabilized (i.e., attained a flat profile) with polymer breakthrough at about
2 2.5 pore volumes injected. The absence of mechanical entrapment could be one plausible
3 explanation for the ‘flat trend’ in the pressure records after breakthrough. The foregoing
4 probably suggests adsorption as the main retention mechanism in these cases.

5



6

7 Fig. 5 – Profile of pressure drop vs. pore volumes injected at different flow rates. FP3630 S
8 HPAM concentration is kept constant at 500 ppm

9

10 3.2 Flow rate dependent retention

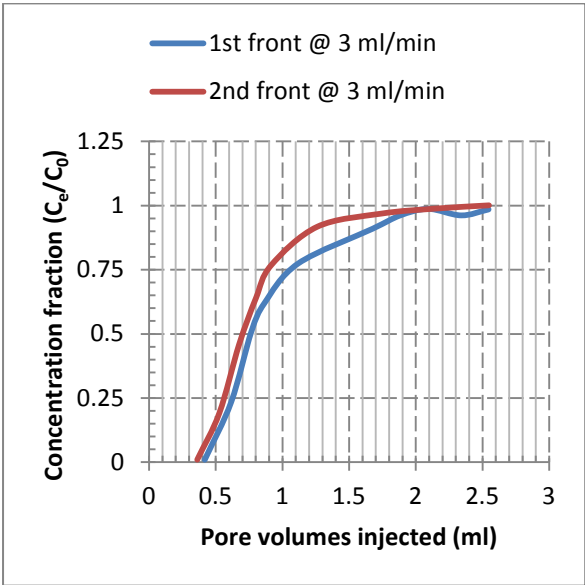
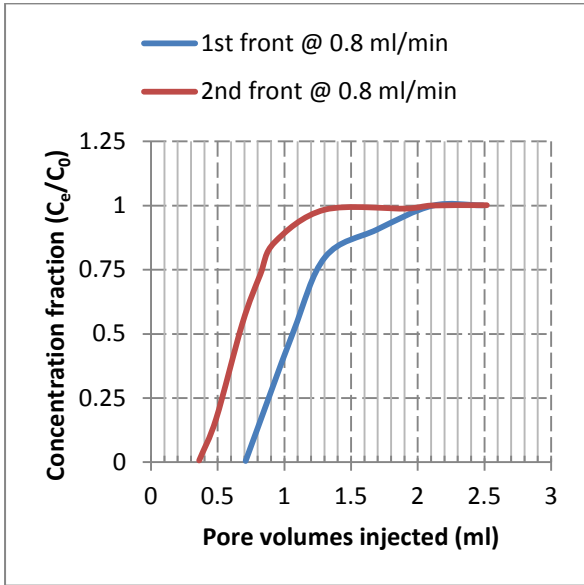
11 **Fig. 6 (a-c)** shows plot of the concentration profiles vs. pore volumes injected for a 500 ppm
12 SNF Flopaam 3630 S HPAM in commercial 348 mD 20/40 sandpack using 3.2% TDS brine.
13 The polymer injections were performed at 0.8 ml/min, 3.0 ml/min and 6.0 ml/min
14 respectively. The breakout curves for both the low and higher rates injection cycles are
15 plotted. In the low flow rate (0.8 ml/min) case, a further shift to higher pore volumes injected
16 at breakthrough is observed; indicating a high retention in the accessible pore volume
17 requiring about 2.5 PVs to reach its injected concentration in the effluent. It is probably due
18 to entrapment in smaller openings between pores and adsorption in the entire core that
19 resulted in higher polymer loss in this case. Furthermore, mass separations between polymer
20 molecules (i.e., smaller molecules have penetrated the pores and were retained) and

1 adsorption kinetics are perhaps, responsible for the spread-out aspect of the polymer front in
2 the low flow rate regime. The fundamental principle of the double-polymer bank method
3 used in this study is that the period of extended brine flush should rinse any reversibly
4 retained polymer from the core or sandpack; and if this retention reoccurred during the
5 following or second polymer flood, then the second effluent concentration profile will move
6 closer to the first one (i.e., shift to the right) as observed in the higher injection rate cases. In
7 this way, only irreversible retention is measured by means of this dynamic method while
8 reversible retention is excluded. In each rate in general, polymer effluent stream
9 concentration continually increased from the injection of about 1 to 2.5 PVs; indicating that
10 some polymer was being retained in the core. Even then, a closer look at the curves for each
11 rate shows that the polymer front reaches its injected concentration after injection of about
12 2.5 PVs; indicating that any polymer loss was dominantly due to an adsorption mechanism
13 for these cases.

14

15 Therefore assuming the absence of all other sources of retention other than adsorption, the
16 difference in area between curves (or the difference in breakthrough between the two
17 polymer fronts) during each of the low and high rate injections gives a measure of the amount
18 of polymer adsorbed. Any adsorption resulting from flow rate increase was then calculated
19 from the difference between the 2nd breakout curve at the first low rate and the 1st breakout
20 curve associated with the subsequent increased flow rates.

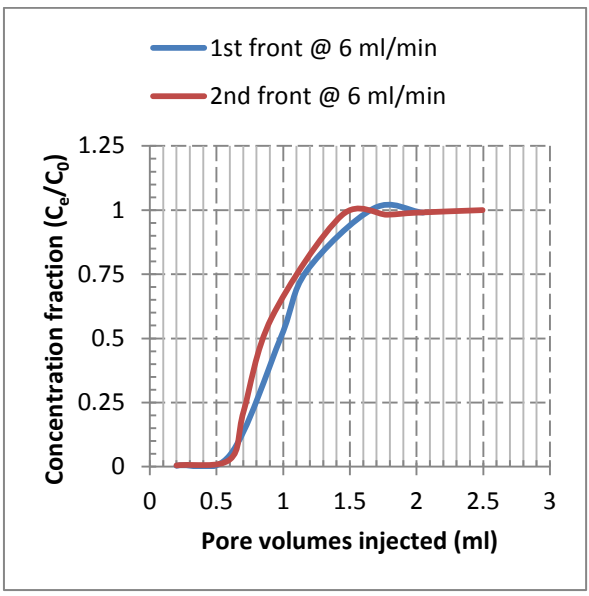
21



1
2

(a)

(b)



3
4
5
6
7
8

(c)

Fig. 6. Rate-dependent retention behaviour of FP3630 S HPAM on silica sand: (a) during low rate injection cycle (0.8 ml/min), (b) during the first high rate injection cycle (3 ml/min), (c) during the second high rate injection cycle (6 ml/min).

1 3.3 Reversible and irreversible polymer adsorption

2 To quantify the effect of rate variation on adsorption in terms of reversible and irreversible
3 total incremental adsorption, adsorption was first measured at low rate of 0.8 ml/min by the
4 special method described earlier, where a value of 0.36 PV (27.32 $\mu\text{g/g}$) was observed. In
5 order to determine flow-rate-induced adsorption, the experiments with 3.0 ml/min and 6.0
6 ml/min were done on the same core as 0.8 ml/min using the same 500 ppm SNF Flopaam
7 3630 S HPAM; with each slug separated by sufficient brine to rinse the “core” of all non-
8 adsorbed polymers after injection at the elevated rates.

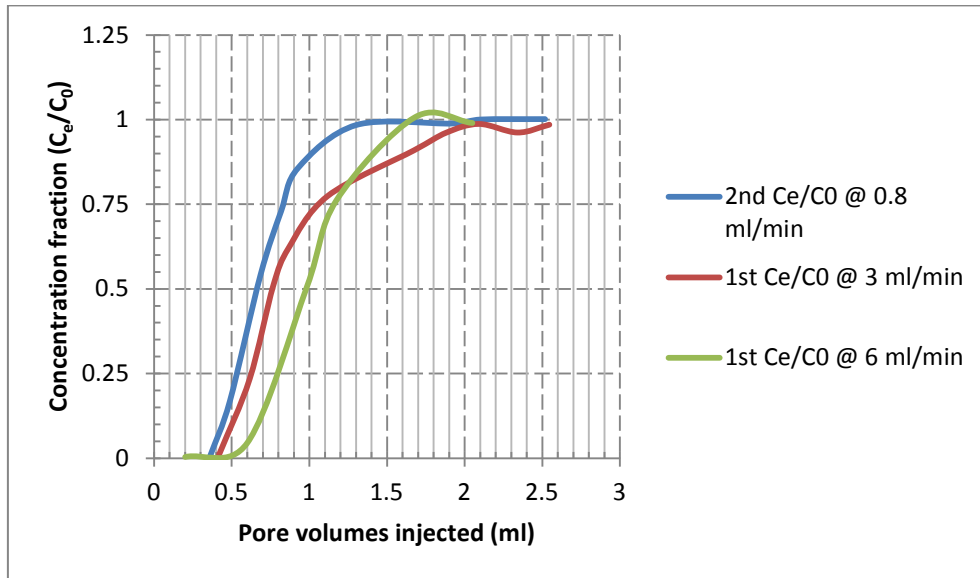
9
10 Plots of the effluent profiles show that the magnitude of the area between the 2nd breakout
11 curve at low rate and the 1st breakout curve at the subsequent higher rates was greater than
12 zero (i.e., no overlay) (**Fig. 7**). The total incremental adsorption induced by this rate variation
13 was determined by the difference in polymer breakout between 2nd breakout curve at low rate
14 (0.8 ml/min) and 1st breakout curves at any subsequent higher injection rates (i.e., 3 and 6
15 ml/min). In principle the double-polymer bank dynamic method presume that during the 1st
16 flood, most of the polymer adsorption demand had been supposedly satisfied. And because
17 the same core was used for all rates, any total incremental adsorption was then calculated by
18 comparing 2nd breakthrough curve at low rate with 1st breakthrough curve at high rate, etc.
19 For these cases, the total incremental adsorption (reversible and irreversible) was calculated
20 to be 0.087 PV at 3 ml/min and 0.304 PV at 6 ml/min (**Fig. 7**). The incremental reversible
21 adsorption was determined by the difference in breakouts between 2nd breakout curves at
22 higher rates (3 and/or 6 ml/min) and 2nd breakout curve at low rate (0.8 ml/min); this gives
23 0.04 PV at 3 ml/min and 0.17 PV at 6 ml/min; while incremental irreversible adsorption was
24 determined by the difference in breakouts between two polymer fronts at each higher rates (3
25 and/or 6 ml/min); this gives 0.047 PV at 3 ml/min (**Fig. 6b**) and 0.134 PV at 6 ml/min (**Fig.**

1 **6c)** This result shows that during the first high rate injection stage at 3 ml/min the additional
2 polymer adsorbed was presumably desorbed; hence the incremental retention for this case
3 was nearly all reversible. The next higher injection stage at 6 ml/min shows higher total
4 incremental adsorption. It is suspected that more brine flush could have driven this to lower
5 value.

6
7 **Fig. 6a** shows that the viscous polymer reached the end of the core after about 1.059 PV
8 during the first cycle of polymer injection and after about 0.68 PV during the second front at
9 0.8 ml/min. Assuming polymer adsorption sites were satisfied during the first injection front
10 in this case; the front arrival of 0.68 PV during the 2nd stage implies an IAPV of 0.32 (i.e., 1-
11 0.68). By similar inferences, IAPV was calculated as 0.28 at 3 ml/min and 0.15 at 6 ml/min
12 respectively (**Figs. 6-8**). Therefore, IAPV is observed to decrease with increasing polymer
13 adsorption; because, at higher rates of injection, the unswept region that is pre-dominated by
14 brine can be penetrated by the polymer solution leading to a decrease in IAPV. This means
15 that increase in flow rate may cause decrease in IAPV; resulting in an increase in polymer
16 adsorption which can also cause delay in polymer propagation rate. These results indicate that
17 IAPV decreased as flow rate increased; the overall consequence being the additional loss of
18 polymer chemicals.

19

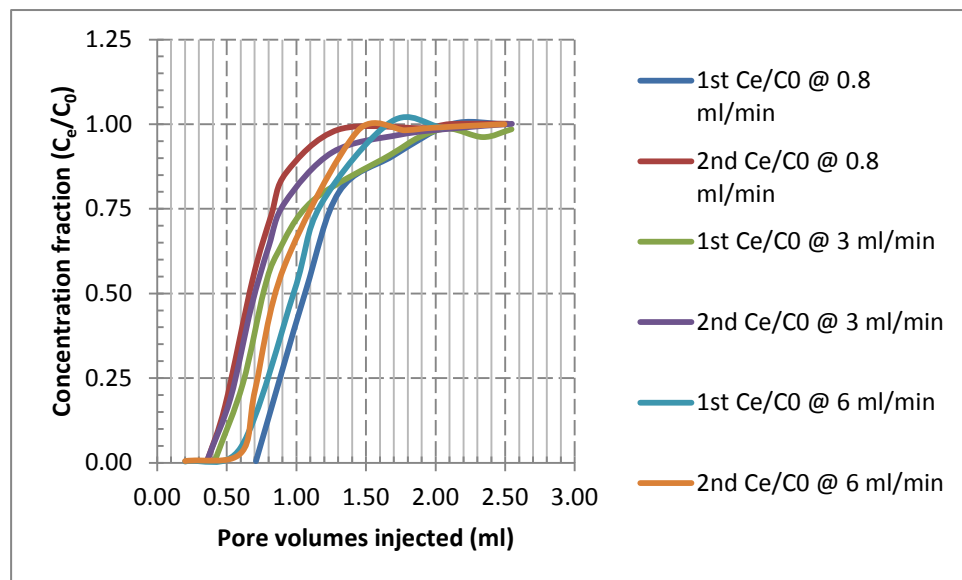
20



1 Fig. 7. Concentration profiles of 500 ppm FP3630 S at 0.8 ml/min, 3 ml/min and 6.0 ml/min.

2

3



4

5 Fig. 8. Plot of concentration profiles of the dynamic method for the study of the effect of flow
6 rate on polymer adsorption for all flow rates investigated.

7

8

9

10

1 **3.4 Permeability reduction investigation**

2 The pressure drop data recorded when polymer was no longer detectable in the effluent
3 stream were converted and used to compute the residual resistance factor (RRF) at the
4 various flow rates. The RRF is a measure of permeability reduction (R_k). Permeability
5 reduction (R_k) defines water mobility before and after polymer flow. It is used to describe
6 reservoir permeability reduction after polymer flooding due to adsorption. Equation 4 is used
7 (Ali and Barrufet, 2001).

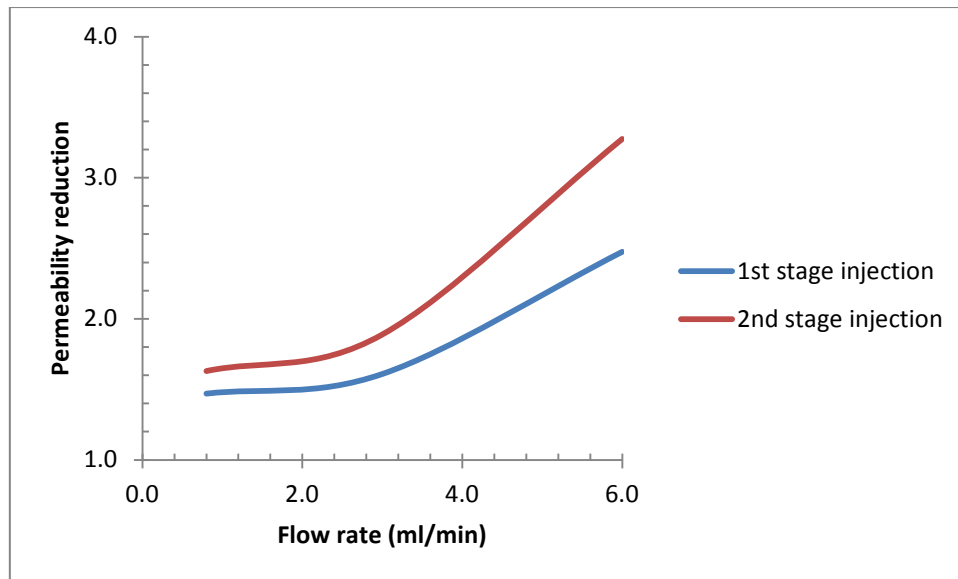
8
$$RRF = R_k = \frac{(\Delta P / Q)_w}{(\Delta P / Q)_{w0}} \quad (4)$$

9 ΔP_{w0} = pressure drop during brine flow before polymer injection (at a certain flow rate, Q).

10 ΔP_w = pressure drop during brine flow after polymer injection (at a certain flow rate, Q).

11

12 **Fig. 9** presents the RRF data taken over the range of flow rate investigated for both stages of
13 polymer displacements. It is clearly shown from the plot that the resistance effect produced
14 by polymers increases as the permeability decreases. The persistent reduction of the pack
15 permeability by HPAM on the other hand is due to polymer chemical adsorption influenced
16 by increasing flow rates. As flow rate is increased, the resultant increase in hydrodynamic
17 forces favours the penetration of new macromolecules in pore walls. This, in turn, increases
18 polymer adsorption; and then, a consequent strong effect on permeability reduction (Fig. 9).
19 The detailed mechanism of this process is explained in section 3.5 below.



1

2 Fig. 9 –Permeability reduction behaviour of 500 ppm FP3630 S HPAM at different flow rates

3

4 **3.5 Polymer induced formation damage**

5 The above results can be used to explain polymer-induced formation damage. Assuming the
6 absence of pore bridging because of the large pore size of the commercial sands used in the
7 experiments, starting with the low rate ensure that adsorption occurred without any additional
8 force except that owing to Brownian motion. To explain this, hydrodynamic forces are too
9 small at low rate to influence polymer macromolecular conformation so that the adsorbed
10 polymer could be described in a similar manner to the “static” adsorption condition; this leads
11 to constant adsorbed layer thickness as expected for the low flow rate case. As the flow rate
12 increases, the resultant increase in hydrodynamic forces supports the invasion of new
13 macromolecules inside the previous “static adsorption” layer, and consequently increases the
14 magnitude of adsorption notwithstanding the existing osmotic barrier. In this way, the
15 adsorbed macromolecular density increases. Because hydrodynamic forces are greatest at the
16 pore throat (where they form secondary flows), a strong effect of permeability reduction
17 (formation damage) is observed in this region. However, these results seem compatible with
18 the permeability level and the quartzitic nature of the sand used for these cases. Overall, these

1 experimental results show that adsorption of polymer was impacted by flow rate. For this set
2 of experimental conditions, it was also observed rate-dependency of polymer adsorption
3 reveals that nearly all the total incremental adsorption was reversible. Although Maerker
4 (1973) and Dominguez and Willhite (1977) obtained similar results, the method and results
5 presented here give a better understanding of reversibility of adsorption and enable the
6 quantification of the flow rate effects on adsorption.

7

8 **5. Conclusions**

- 9 1. Using HPAM polymer solution and well characterized model granular sand pack, a
10 quantitative study of flow rate-dependent polymer adsorption is explained with the aid of
11 data from core flood experiments.
- 12 2. The double-polymer bank dynamic method was adopted; and the experimental findings
13 show that adsorption is the only source of polymer retention for the range of flow rates
14 investigated.
- 15 3. Results show that adsorption of polymer was impacted by the variation in flow rate. For
16 the cases investigated, rate influence of polymer adsorption reveals that nearly all the total
17 incremental adsorption was reversible with minimal irreversibility.
- 18 4. The results also show that IAPV decreases (from 32 to 15%) as flow rate increases; the
19 consequence being the additional loss of polymer chemicals.
- 20 5. Previous studies (e.g., Maerker, 1973; Huh et al., 1990; Dominguez and Willhite, 1977)
21 obtained similar results mostly with xanthan gum. The permeability reduction factor of
22 xanthan gum is not significant. Therefore, the method and results presented here give a
23 better understanding of total incremental HPAM adsorption (both reversible and
24 irreversible) induced by flow rate. Further, results from the study give better insight into
25 HPAM flow-induced adsorption and their effect on permeability reduction.

1

2 **Acknowledgement**

3 The authors gratefully acknowledge Petroleum Technology Development Fund (PTDF)
4 Nigeria, for funding the PhD work from which the materials presented in this paper were
5 derived.

6

7 **References**

- 8 Ali, L., Barrufet, M., 2001. Using centrifuge data to investigate the effects of polymer
9 treatment on relative permeability. *Journal of Petroleum Science and Engineering*,
10 29(1), pp. 1-16.
- 11 API. 1990. API RP 63 Recommended Practices for Evaluation of Polymers Used in
12 Enhanced Oil Recovery Operations. American Petroleum Institute, Washington, D.C.
13 June 1990.
- 14 Aubert, J., Tirrell, M., 1980. Flows of dilute polymer solutions through packed porous
15 chromatographic columns. *Rheologica Acta* 19(4), 452-461.
- 16 Chauveteau, G., Denys, K., Zaitoun, A., 2002. New insight on polymer adsorption under high
17 flow rates. Paper SPE 75183-MS presented at the SPE/DOE symposium on Improved
18 Oil Recovery, Tulsa, Oklahoma, USA, 13-17 April.
- 19 Dang, T.Q.C., Chen, Z.J., Nguyen, T.B.N., Bae, W., 2014. Investigation of isotherm polymer
20 adsorption in porous media. *Petroleum Science and Technology*, 32(13), pp.1626-
21 1640.
- 22 Dominguez, J., Willhite, G., 1977. Retention and flow characteristics of polymer solutions in
23 porous media. *Society of Petroleum Engineers Journal*. 17(02), 111-121.
- 24 Hughes, D.S., Teew, D., Cottrell, C.W., Tollas, J.M., 1990. Appraisal of the use of polymer

1 injection to suppress aquifer influx and to improve volumetric sweep in a viscous oil
2 reservoir. SPE Res Eng. 5(1), 33-40.

3 Huh, C., Lange, E., Cannella, W., 1990. Polymer retention in porous media. SPE/DOE
4 Enhanced Oil Recovery Symposium, Tulsa, Oklahoma, 22-25 April.

5 Lake, L.W., Johns, R.T., Rossen, W.R., Pope, G.A., 2014. Fundamentals of enhanced oil
6 recovery. Society of Petroleum Engineers, Richardson, TX, USA, ISBN: 978-1-
7 61399-407-8.

8 Lotsch, T., Muller, T., Pusch, G., 1985. The effect of inaccessible pore volume on polymer
9 coreflood experiments. Paper SPE 13590 presented at the SPE Oilfield and
10 Geothermal Chemistry Symposium, Phoenix, Arizona, 9-11 April.

11 Maerker, J., 1973. Dependence of polymer retention on flow rate. J. Pet. Technology. 25(11),
12 1307-1308.

13 Osterloh, W., Law, E., 1998. Polymer transport and rheological properties for polymer
14 flooding in the North Sea Captain field. Paper SPE 39694 presented at the SPE/DOE
15 Improved Oil Recovery Symposium, Tulsa, Oklahoma, USA, 19-22 April.

16 Pefferkorn, E., Nabzar, L., Carroy, A., 1985. Adsorption on polyacrylamide to Na kaolinite:
17 correlation between clay structure and surface properties. Journal of colloid and
18 interface science, 106(1), 94-103.

19 Yerramilli, S.S., Yerramilli, R.C., Zitha, P.L.J., 2013. Novel insight into polymer injectivity
20 for polymer flooding. Paper SPE 165195-MS presented at the SPE European
21 formation conference and exhibition, Noordwijk, The Netherlands, 5-7 June.

22 Zitha, P., Chauveteau, G., Zaitoun, A., 1995. Permeability-dependent propagation of
23 polyacrylamides under near-wellbore flow conditions. Proceedings of the
24 International symposium on oilfield chemistry. pp. 101-116.